Application of Micromechanics on Alkali-activated Materials

Vít Šmilauer[1, a], František Škvára[2, b], Jiří Němeček[1, c], Lubomír Kopecký[1, d], Petr Hlaváček[1, e]

[1]Czech Technical University in Prague, Faculty of Civil Engineering, Department of Mechanics, Thákurova 7, 166 29 Prague, Czech Republic

[2]Institute of Chemical Technology Prague, Department of Glass and Ceramics, Technická 5, 166 28 Prague, Czech Republic

[a]vit.smilauer@fsv.cvut.cz, [b]frantisek.skvara@vscht.cz, [c]jiri.nemecek@fsv.cvut.cz, [d]kopecky@fsv.cvut.cz, [e]petr.hlavacek.1@fsv.cvut.cz

Keywords: Nanoindentation, N-A-S-H gel, fly ash, metakaolin, micromechanics, elasticity, homogenization

Abstract. Research of alkali-activated materials has been a traditional domain of chemists. This paper exploits contribution of micromechanics to the subject. Alkali-activation of the fly-ash is perceived as the volumetric evolution of elastically-invariant components. Nanoindentation technique identified the intrinsic Young's modulus of N-A-S-H gel as ~18 GPa, which was further downscaled to the solid gel particles. Percolation theory applied to N-A-S-H gel was introduced to cover an early-age elasticity. Combination of the two-scale elastic homogenization method, percolation theory and intrinsic elastic properties of components show a good reproduction of experimental data obtained from the macroscale. Homogenization model also demonstrates the stiffening of N-A-S-H gel, induced by increased packing of the solid gel particles.

Introduction

A group of alkali-activated aluminosilicate materials draws the attention of researchers worldwide, see [1,2] for a comprehensive review. In comparison with conventional Portland cement-based composites, these materials generally exhibit excellent durability, fire-resistance, but may suffer from efflorescense, shrinkage, cumbersome quality control or mastering the technology [3,4].

In the past, various raw materials (slag, fly-ash, metakaolin, clay) were intermixed with strong alkaline solutions to synthesize a poorly crystallized inorganic gel binder [5]. Coined nomenclatures such as “soil cement” [6], “geopolymer” [7] or “inorganic polymer” [2] have characterized more or less similar dissolution-precipitation processes taking place in a strong alkaline environment due to different starting materials. Here, the term N-A-S-H gel (aluminosilicate gel) will describe a binding matrix phase, embedding undissolved inclusions of a remaining raw material.

In the past, alkali-activated materials were characterized by a variety of experimental techniques including FTIR, ESEM, MAS-NMR, XRD, DTA or calorimetry [4,5]. The majority of experimental data were linked directly to the atomic scale and nanostructure of N-A-S-H gel. However, all the above mentioned techniques suffer from data downscaling by several orders of magnitude to the nanostructure of N-A-S-H gel. In this sense, a traditional chemical description of alkali-activated materials may be enriched with micromechanics, as proven successfully for the description of Portland-based materials [8,9].

Micromechanical elastic analysis stems from the definition of intrinsic elastic properties of constituents. These are considered to remain independent on ongoing chemical reactions with possible evolution of volume fractions during the alkali-activation. Nanoindentation sensing

technique enables direct characterization of intrinsic mechanical properties on the micrometer and submicrometer resolution. The response is obtained directly from a close vicinity of a small indent without the interaction of distant material. Such measurements have never been performed systematically in this field, although a few attempts can be found [10].

This paper aims at interconnecting chemical and mechanical disciplines. First, intrinsic elastic properties are identified from alkali-activated fly ash (AAFA) and alkali-activated metakaolin (AAMK). Second, a new volumetric model of alkali activation is formulated. Third, two-scale elastic homogenization combined with percolation upscales the intrinsic properties to the macrospopic scale.

Materials, Alkali-activation and Curing

The raw fly ash (RFA) was produced in Chvaletice thermal electric power plant, Czech Republic, with the Blaine specific surface 210 m^2kg^{-1}. For nanoindentation, RFA was ground in a small-scale ball mill in the quantity of 8 kg for 180 minutes to crush cenospheres in order to reduce the porosity. Metakaolin originated from České lupkové závody a.s., Nové Strašecí, Czech Republic. Chemical compositions of both materials are summarized in Table 1.

Table 1. Chemical composition of fly ash and metakaolin, wt. %.

	SiO_2	Al_2O_3	Fe_2O_3	CaO	TiO_2	K_2O
Fly ash	51.9	32.8	6.3	2.7	1.89	2.12
Metakaolin	48.66	47.41	1.33	0.03	1.99	0.15

The alkali-activator was previously optimized to yield a high compressive strength while maintaining workability [4]. The activator was prepared by dissolving NaOH pellets in tap water and adding sodium waterglass. Table 2 summarizes the compositions of the mixtures. The final properties of the mixture can be controlled by three independent parameters, see Table 2. Metakaolin requires significantly more activator due to its higher surface area to maintain a reasonable workability.

Table 2. Composition of alkaline activators and ratii to the activated material.

	Activator ratii		Activator to solid ratio (wt. %)
	Na_2O / SiO_2 (wt. %)	H_2O / Na_2O (wt. %)	
Ground fly ash	0.881	3.925	0.531
Metakaolin	1.669	2.743	1.416

Fly ash or metakaolin was intermixed with the activator for 5 minutes, cast in plastic ampules, 26 mm in diameter and 45 mm in height, gently vibrated for 5 minutes and sealed. Heat-cured fly ash or metakaolin samples were exposed to 80^{o}C for 12 hours. Ambient-cured fly ash experienced a laboratory temperature, approx. 25^{o}C, for the duration of six months prior to nanoindentation testing. Both materials are considered to be mature, although polymerization and hardening will never stop as known from C-S-H aging [11]. After a half-year from casting, the compressive strength of AAFA samples exceeded 70 MPa and 50 MPa of AAMK.

Methods

Nanoindentation. Activated samples were cut to parallel slices of approx. 10 mm in thickness, polished on fine emery papers and polishing cloth, and cleaned in an ultrasonic bath.

Nanoindentation was carried out in a series of grids of 10 x 10 = 100 imprints in three representative areas. The distance between individual indents varied between 10 and 50 \um.

Nanoindentation measurements were performed in a load control regime using the CSM Nanohardness tester equipped with a Berkovich tip. The trapezoidal loading diagram was prescribed for all tests with linear loading of 4 mN/min and lasting for 30 s, which produced a maximum load of 2 mN for all indents. Peak load of 2 mN led to maximum penetration depths ranging from 100 nm to 400 nm. Fig. 1 shows a typical force/penetration diagram for three identified material phases.

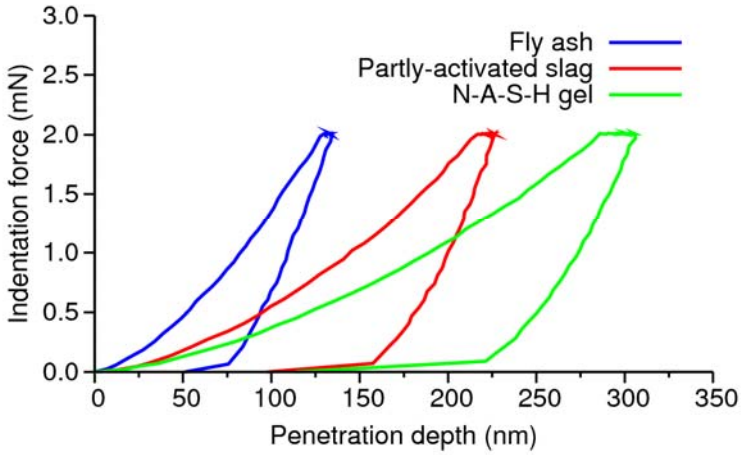

Figure 1. A typical nanoindentation diagram for alkali-activated fly ash.

The effective depth captured by the tip of the nanoindenter can be roughly estimated as three to four times of the penetration depth for the Berkovich indentor [12]. It yields the effective depth of around 1 \um from which the elasticity is obtained.

Determination of Open Porosity. Cylindrical samples (diameter 25 mm, thickness 5 mm) of a well-defined geometry were dried out in an oven at 105°C. Samples remained in the oven environment until the weight loss stabilized, which took from 3 to 6 days. Known skeletal density of fly ash from He pycnometry, known skeletal density of activate fly ash and known sample volume led to quantification of the open porosity. The open porosity was determined from three samples and the experiments were repeated during ambient curing of alkali-activated materials to access the evolution of open porosity.

Results and Discussion

Degree of Reaction. The degree of reaction, DoR, is defined as the amount of consumed fly ash in the alkali-activation process. Direct simulation of DoR from a known chemical composition is beyond capabilities of presented models, which do not include reaction kinetics. Instead, the evolution of DoR is taken from experimental data of Fernández-Jiménez et al. [13] who measured a progress of reaction degree on AAFA samples activated with 8 M NaOH solution and cured at 85°C. The extent of DoR was determined by an acid attack with HCl 1:20. Similar results were observed on calorimetry data, which revealed that the ratio activator/fly-ash is insignificant for the DoR and that a maximum reaction rate occurs at 8-10 minutes after the contact, ending up to 2 hours at elevated temperatures [14].

Arrhenius equation is utilized to recalculate DoR for various constant temperatures of curing. For example, the time scaling from 60°C to 20°C means a slow down 70-times. The Arrhenius equation reads

$$\tau(T_{20}) = \tau(T_{60}) \exp\left[\frac{E_a}{R}\left(\frac{1}{T_{20}} - \frac{1}{T_{60}}\right)\right]$$

, (1)

where the activation energy was found 86.2 kJ/mol [4]. The transition from 85°C to 25°C predicts the scaling factor 340. Fig. 2 shows the DoR evolution at 25°C, recalculated from [13].

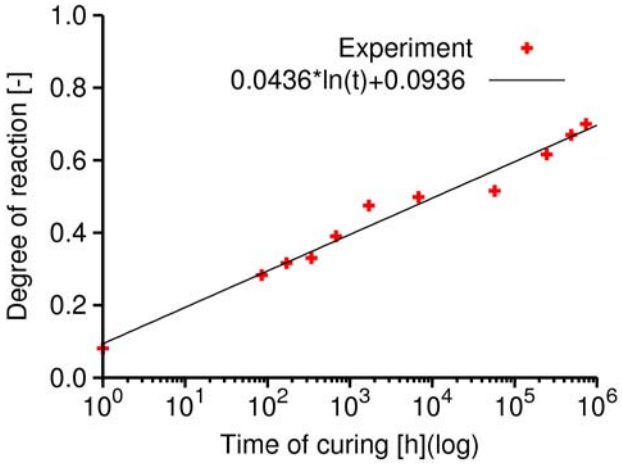

Figure 2. Progress of DoR for alkali-activated fly ash by 8M NaOH. The evolution of DoR is showed at a reference temperature of 25°C. Original data gathered at 85°C came from [13].

Porosity and ESEM. AAFA and AAMK samples were crushed to the size of a few millimeters, dried at 105°C for 6 hours and intruded by mercury (MIP, Autopore III Micromeritics) or measured by He-pycnometry (Micromeritics AccuPyc 1330). The combination of MIP and He pycnometry allowed estimating the "total" porosity from bulk and skeletal densities. The porosity captures the range from a helium atom (d=0.062 nm) from the bottom range and the limit of MIP from the top (d=120 \um). The pore size distribution obtained from MIP and He pycnometry is depicted in Fig. 3; for ordinary Portland cement paste and for alkali-activated samples.

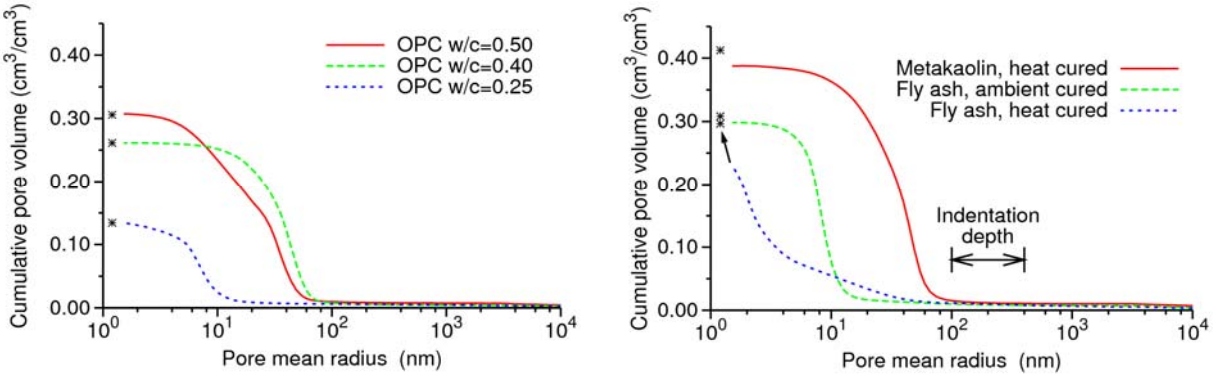

Figure 3. Cumulative pore volume by MIP and He pycnometry. OPC paste cured at 60°C for three months (left) and alkali-activated materials (right). An asterisk denotes the total volume derived from from the size of a helium atom.

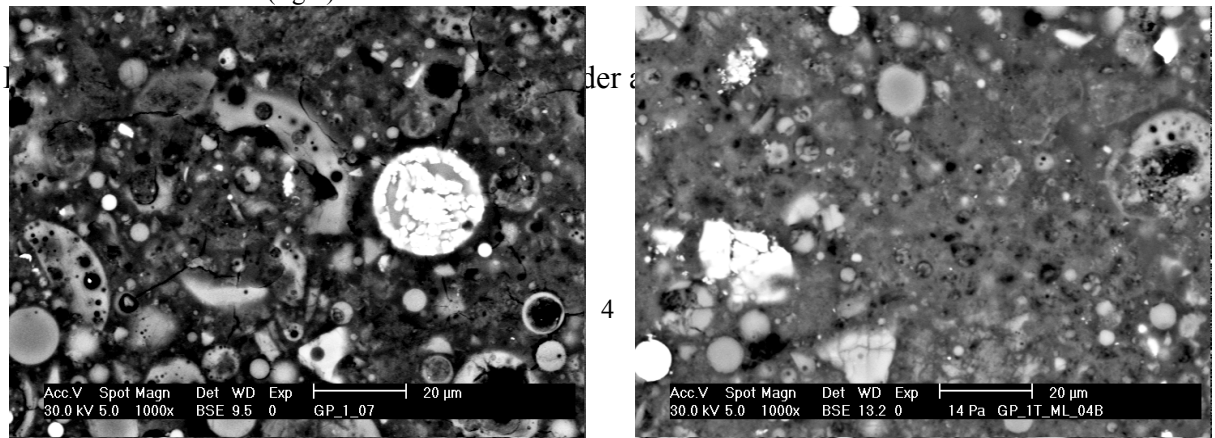

Figure 4. BSE images of AAFA cured under ambient conditions (left) and cured at 80°C for 12 hours (right).

Identification of N-A-S-H gel's elastic properties and a solid gel particles. Indentation moduli from 700 locations were gathered and recalculated to Young's moduli. The moduli were processed statistically to a histogram. Fig. 5 shows the histogram with a deconvolution to four Gaussian distributions. Deconvolution is generally an ill-posed problem and many solutions exists, however, the peak for N-A-S-H is clearly and unambiguously defined. Other phases are hypothesized to present partly-activated slag and unreacted material.

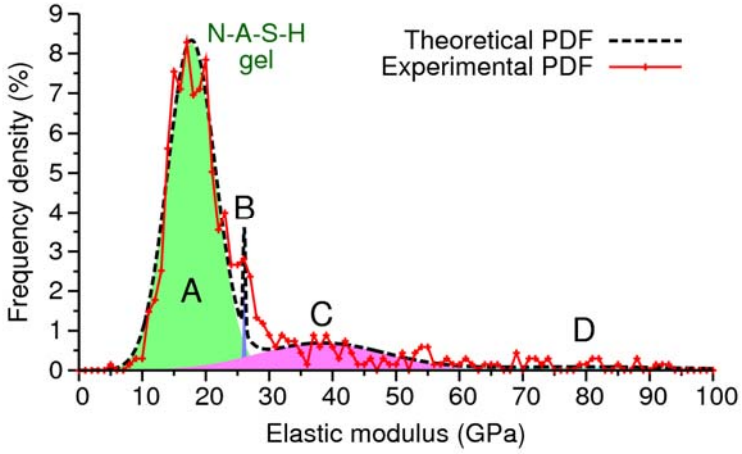

Figure 5. Overall experimental and theoretical probability density functions with segmented four phases in ambient-cured AAFA samples. Peak are hypothesized to mean A - N-A-S-H gel, B - Partly-activated slag, C - Nonactivated slag, D - Nonactivated compact glass.

Deconvolution for heat-cured AAFA and AAMK samples yielded similar Young's moduli for N-A-S-H gel. Table 3 summarizes N-A-S-H gel moduli together with corresponding volume fraction from the histogram. Volume fraction of N-A-S-H gel in the heat-cured AAFA is lower due to significant presence of peak B (not showed). Coincidence of the same moduli among different alkali-activated materials and curing procedures proves the same intrinsic elastic properties of N-A-S-H gel, irrespective of its origin.

Table 3. Elastic moduli of N-A-S-H gel synthesized from different precursors.

	Ambient-cured AAFA	Heat-cured AAFA	Heat-cured AAMK
Young's modulus of N-A-S-H gel	17.72 ± 3.75 GPa	17.03 ± 3.48 GPa	17.72 ± 4.43 GPa
Volume fraction from histogram	77.50%	50.70%	97.20%

The histogram in Fig. 5 shows no porosity, which should be at least 30 % according to Fig. 3. As evident from Fig. 3, nanoindentation imprint is much larger than a fine porosity, which is scattered within a sample. A minor part of porosity is apparently present in the fly ash (cenospheres, plerospheres) and the major part inside the N-A-S-H gel.

Any sol-gel system consists of solid particles dispersed in a liquid [15]. Sol-gel is far from equilibrium and solid particles may aggregate into clusters. If condensation reaction in the system exists and is irreversible, more and more solid particles appear in the system and grow into fractals [15]. Linking of clusters continues until they reach a percolation threshold signalized by a sudden change of many properties such as elasticity.

C-S-H gel in rather a precipitate than a gel due to the presence of capillary pores and inability to fill uniformly the space. Reversible condensation reaction dominates C-S-H solidification [15]. Another consequence of reversibility is a constant 28% porosity of the C-S-H gel, irrespective of an origin or time under normal curing condition [16]. The constant porosity allowed to consider C-S-H gel as one phase from a micromechanical point of view; solid particles intermixed with the porosity at the same fraction.

N-A-S-H is a true gel which fills out all available volume. Gel syneresis has been observed many times in alkali-activated materials; excessive shrinkage accompanied with a strong sample disintegration might have occurred under the sealed conditions. Due to a true gel nature, no constant gel porosity, as in the C-S-H, exists and the micromechanical response needs to be determined from the solid gel particles. The intrinsic elastic properties of the particles are carried out by a downscaling process. Knowing the elasticity of the N-A-S-H gel and the amount of porosity, one may determine unknown intrinsic elasticity of the solid gel particles.

Volumetric Model for Alkali-activation. Volumetric model for alkali-activation presents a stepping stone for the micromechanical analysis. Much inspiration has been gathered from Portland cement, starting from maturity method [17] and continuing through a famous research carried out by Powers and Brownyard [16]. Fig. 6 shows volumetric plots for both Portland cement and alkali-activated fly-ash. Four chemically and mechanically distinctive phases needed to be identified and described in the alkali-activated fly ash.

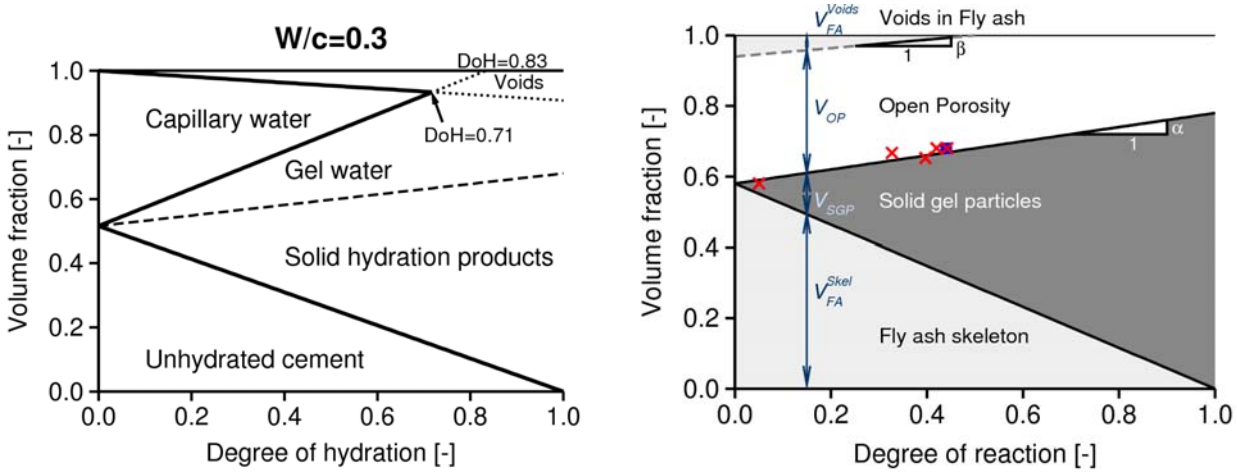

Figure 6. Comparison between famous Powers' model for hydrating Portland cement and a newly proposed model for alkali activation of fly ash.

V_{FA}^{Skel} represents the volume fraction fly-ash skeleton. Voids persisting in the fly-ash after the mixing are quantified with V_{FA}^{Voids}. It must be noted that after a few minutes during the mixing, the activator efficiently destroys a thin shell of plerospheres and opens their porosity. This is manifested by a partial loss of workability and heat release in isothermal calorimetry. Voids in the fly ash were obtained from the combination of known skeletal density of fly ash, density of activating solution and measured volume and weight of mixture immediately after the mixing process.

V_{SGP} is the volume fraction of solid gel particles. The term "N-A-S-H gel" is intentionally unused due to the gel composition from solid and liquid parts. No characteristic gel porosity exist, hence the gel could be treated as the activator plus the solid gel particles. Volume of open porosity,V_{OP}, describes conveniently a part of accessible porosity by external water. The activator fills up the major part of open porosity.

Degree of reaction (DoR) presents a microstructural parameter, which describes the alkali-activation progress of the fly ash. Expressing all reactions in terms of DoR is more convenient against time for two reasons:

- Circumventing a logarithmic time scale, needed for a proper plot.
- Mutual comparison for samples cured at various temperatures.

No fly ash becomes activated and consumed at DoR = 0.0, while a complete activation occurs at DoR = 1.0. To build a simple conceptual model describing basic phenomena, several assumptions of the volumetric model had to be made:

- The whole activator is treated in the form of evaporable water, disregarding a small solid part remaining after drying. Under saturation, open porosity is filled with evaporable water.
- No chemical shrinkage/expansion occurs so that the volumetric balance of all liquid and solid phases is maintained during the activation progress.
- All reactions are time-independent and depend only on DoR. Such simplification neglects separate contribution of dissolution, precipitation and aging of N-A-S-H gel.

$$V_{FA}^{Skel}(\mathrm{DoR}) = V_{FA}^{Skel}(0)\,[1-\mathrm{DoR}]\,, \tag{2}$$

$$V_{FA}^{Voids}(\mathrm{DoR}) = V_{FA}^{Voids}(0) - \beta\mathrm{DoR},\ V_{FA}^{Voids}(\mathrm{DoR}) \geq 0, \tag{3}$$

$$V_{SGP}(\mathrm{DoR}) = \left[V_{FA}^{Skel}(0) + \alpha\right]\mathrm{DoR}, \tag{4}$$

$$V_{OP}(\mathrm{DoR}) = 1 - V_{FA}^{Voids}(\mathrm{DoR}) - V_{FA}^{Skel}(0) - \alpha\mathrm{DoR}, \tag{5}$$

Parameters for Eq. 2 – Eq. 5 had to be obtained experimentally. The section Methods describes the assessment of open porosity in the AAFA. V_{FA}^{Voids} disappear roughly at the DoR=0.5. Table 4 summarizes fitted parameters for the volumetric model. This conclusion is supported with isooctane saturation of dried-out samples. The method is described in [18] and is not showed.

Table 4. Fitted parameters for the volumetric model of alkali-activation.

Parameter	Fitted value, see Fig. 5
$V_{FA}^{Skel}(0)$	0.58
$V_{FA}^{Voids}(0)$	0.06
$V_{OP}(0)$	0.36
alpha	0.2
beta	0.12

Downscaling and two-scale homogenization. Elastic properties of the solid gel particles were obtained by means of a downscaling process. Characterization of N-A-S-H gel by nanoindentation was considered to occur at DoR = 0.44, which gives the volume fractions summarized in Table 5.

Table 5. Volumetric fractions at DoR = 0.44 and elastic properties of constituents.

Parameter	Volume fraction [-]	Young's modulus [GPa]	Poisson's ratio [-]
$V_{FA}^{Skel}(0.44)$	0.324	104.0	0.20
$V_{FA}^{Voids}(0.44)$	0.001	0.001	0.001

$V_{EW}(0.44)$	0.325	0.001	0.499924
$V_{SGP}(0.44)$	0.350	38.2-**49.8**-59.5[a]	0.22-**0.23**-0.24[a]
Sum	1.000		

[a]) Three values stem from a standard deviation of N-A-S-H gel indentation moduli.

First, the solid gel particles and evaporable water were considered to form the N-A-S-H gel. Volumetric fraction of the above-mentioned phases are 0.5185 and 0.485, respectively. Mori-Tanaka scheme for an isotropic spherical inclusion [19] run with the reference phase of the gel particles and identified elastic properties of them, see Table 5. Standard deviation of indentation moduli obtained for the N-A-S-H gel, 17.72 ± 3.75 GPa, see Table 3, led to the variation of elastic properties of the solid gel particles.

Second, elastic properties of AAFA constituents were connected with the volumetric model for alkali-activation. Two-level elastic homogenization seemed to give reasonable results. In the first level, elastic properties of the N-A-S-H gel, composed from the solid gel particles and evaporable water in the open porosity, were obtained using Mori-Tanaka method with the reference phase of the solid gel particles. The second level homogenized the gel, fly ash and voids in the fly ash, by repeating the Mori-Tanaka method with the reference phase of N-A-S-H gel.

Fig. 7 summarizes the results from two-scale homogenization at the level of AAFA. Experimental data came from a non-destructive measurement by cyclic loading. The load level attained approximately 0.3 of ultimate load and the load was applied uniaxially on prismatic samples 40x40x160 mm, equipped with a set of extensometers to control bending induced by the load eccentricity.

Homogenization solely by Mori-Tanaka method shows a big discrepancy in the beginning of alkali-activation process. The reason lies in percolation properties of true N-A-S-H gel. Until a certain point called a percolation threshold, the solid gel particles are mutually separated although the volumetric model predicts their presence. The assumption of perfect bonding, on which the homogenization methods are based, is violated at this stage. Percolation problems are known to occur in early ages of hydration in the system of Portland cement paste [9]. Introducing the percolation function in the form

$$p = (\mathrm{DoR} - \mathrm{DoR}_p), \tag{6}$$

allowed to introduce the percolation threshold DoR_p, from which the N-A-S-H gel's modulus becomes non-zero. The Young modulus from the N-A-S-H gel is multiplied with the Eq. 6. Calibration to the experimental data yielded DoR_p=0.335 and also set the upper limit DoR = 0.405, above which percolation plays no role and sets p = 1.

The thick line in Fig. 7 shows the elastic prediction in terms of average AAFA's modulus. Introducing the scatter in the solid gel particles leads to widening the range of validity and seems to cover almost all experimental points. In addition, self-consistent scheme in Fig. 7 demonstrates that intrinsic percolation threshold associated with the scheme is in reasonable correlation with experimental data. However, later elastic properties via the self-consistent scheme would be seriously underestimated, which denies its application.

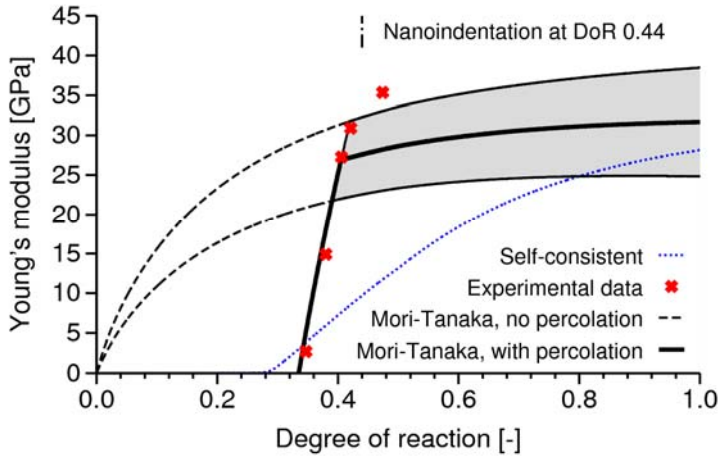

Figure 7. Homogenized elastic properties of alkali-activated fly ash combining the volumetric model, Mori-Tanaka homogenization method and the percolation theory.

Fig. 8 shows elastic results from the first level of N-A-S-H gel. The percolation function gives a negligible elasticity when $DoR_p<0.335$. At the percolation threshold, the volume fraction of the solid gel particles are $V_{SGP}=0.2613$ and of open porosity $V_{OP}=0.3332$. It means that the percolation threshold occurs when the solid gel particles poses a relative volume 0.4395. Rintoul and Torquato [20] performed an extensive numerical study in the system of identical (monodisperse) overlapping spheres, resulting in the percolation threshold 0.2895±0.0005. The percolation threshold changes when a particle size distribution is taken into account. Two distinct sphere diameters were found to have the percolation threshold as high as 0.70 [21].

Note that the N-A-S-H gel is still stiffening due to increasing fraction of solid gel particles. The presented model, based on a packing density of the solid gel particles, does not address changes within the particle, which may occur due to the polymerization on atomistic scale.

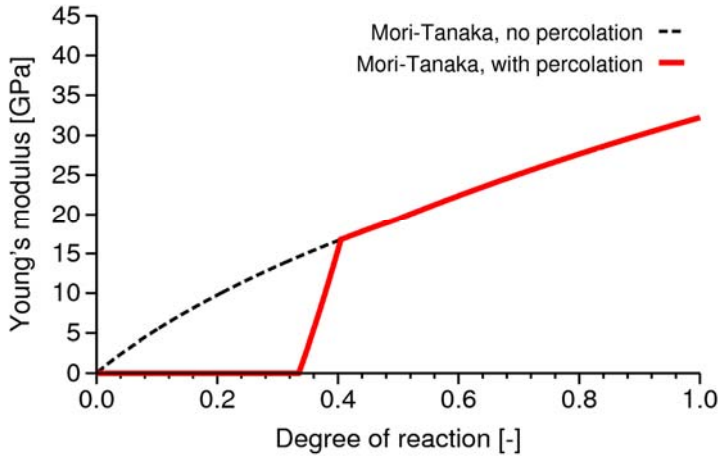

Figure 8. Evolution of Young's modulus within the N-A-S-H gel. Results from the volumetric model, Mori-Tanaka homogenization method and percolation theory.

Conclusions

The combination of nanoindentation, micromechanical modeling and volumetric model provides a different point of view on alkali-activated materials, particularly those made from the fly ash. The N-A-S-H gel is a true gel and the early elastic behavior can be conveniently described with the percolation theory. The models explain several phenomena occurring during the hardening and clarify why the hardening occurs within many days at ambient curing temperature and why the initial and final setting time lay so much far apart. A heat-curing process seems to be a necessity for the production of these materials on a large scale.

The Young's modulus of the N-A-S-H gel (~18 GPa) is quite similar to C-S-H gels (21.7-29.4 GPa) [12]. Beyond the point of chemical compatibility, these gels can also coexist well together from the micromechanical perspective and match of the elastic moduli.

Acknowledgement

Authors gratefully acknowledge the financial support from the Czech Science Foundation, grant 103/08/1639 "Microstructure of inorganic aluminosilicate polymers".

References

[1] F. Pacheco-Torgal, J. Castro-Gomes, S. Jalali: Alkali-activated binders: A review: Part 1. Historical background, terminology, reaction mechanisms and hydration products, Construction and Building Materials Vol. 22 (2008), p. 1305 – 1314.

[2] P. Duxson et al.: Geopolymer technology: the current state of the art, Journal of Materials Science Vol. 42 (2007), p. 2917 – 2933.

[3] C. Shi, P. V. Krivenko, D. Roy: *Alkali-activated cements and concrete* (Taylor & Francis, 2006).

[4] F. Škvára et al.: Material and structural characterization of alkali activated low-calcium brown coal fly ash, Journal of Hazardous Materials Vol. 168 (2009), p. 711-720.

[5] A. Fernández-Jiménez et al.: Immobilization of cesium in alkaline activated fly ash matrix, Journal of Nuclear Materials Vol. 346 (2005), p. 185-193.

[6] V. D. Glukhovsky: *Soil Silicates (Gruntosilikaty)* (Kiev, Budivelnik publisher, USSR 1959).

[7] J. Davidovits: Synthesis of new high-temperature geo-polymers for reinforced plastics/composites, in Proceedings of PACTEC'79, Society of Plastic Engineers (1979), p. 151-154.

[8] O. Bernard, F.-J. Ulm, and E. Lemarchand: A multiscale micromechanics-hydration model for the early-age elastic properties of cement-based materials, Cem. Concr. Res. Vol. 33 (2003), p. 1293-1309.

[9] V. Šmilauer, Z. Bittnar: Microstructure-based micromechanical prediction of elastic properties in hydrating cement paste, Cem. Concr. Res. Vol. 36 (2006), p. 1708-1718.

[10] I. Beleňa, W. Zhu: Nanoindentation Study of Na-Geopolymers Exposed to High Temperatures, in Proceedings of the Nanotechnology in Construction 3, edited by Z. Bittnar et al. (Springer, 2009), p. 169 – 174.

[11] F. Lea, *Lea's Chemistry of Cement and Concrete* (Elsevier 2004).

[12] G. Constantinides et al.: Grid indentation analysis of composite microstructure and mechanics: Principles and validation, Materials Science and Engineering A (2006), p. 189-202.

[13] A. Fernández-Jiménez, A. Palomo, and M. Criado: Microstructure development of alkali-activated fly ash cement: a descriptive model, Cem. Concr. Res. Vol. 35 (2004), p. 1204-1209.

[14] A. Palomo, M. W. Grutzeck, and M. T. Blanco, Alkali-activated fly ashes. A cement for the future, Cem. Concr. Res. Vol. 29 (1999), p. 1323-1329.

[15] G. W. Scherer: Structure and properties of gels, Cement and Concrete Research Vol. 29 (1999), p. 1149 – 1157.

[16] T. C. Powers and T. L. Brownyards: *Studies of physical properties of hardened Portland cement paste*, Bulletin 22 (Chicago: Research Laboratories of the Portland Cement Association 1948).

[17] N. J. Carino and H. S. Lew: *The maturity method: from theory to application* (NIST, 2001).

[18] D. S. Perera: Influence of curing schedule on the integrity of geopolymers, Journal of Materials Science Vol. 42 (2007), p. 3099-3106.

[19] T. Mori and K. Tanaka: Average stress in matrix and average elastic energy of materials with misfitting inclusions, Acta Metallurgica Vol. 21 (1973), p. 1605-1609.

[20] M. D. Rintoul and S. Torquato: Precise determination of the critical threshold and exponents in a three-dimensional continuum percolation model, J. Phys. A: Math. Gen. Vol. 30 (1997), p. 585-592.

[21] S. Torquato: *Random Heterogeneous Materials. Microstructure and Macroscopic Properties* (Springer-Verlag New York, 2001).